Fatigue Damage Development in a Steel Based MMC

V. Tvergaard[1], **T. Ørts Pedersen**[1]

Abstract: The development of fatigue damage in a tool-steel metal matrix discontinuously reinforced with TiC particulates is analysed using a numerical cell model. The material is subjected to cyclic loading, and the matrix material is represented by a cyclic plasticity model, which uses a superposition of kinematic and isotropic hardening, with continuum damage mechanics incorporated to model fatigue damage evolution. The cell model represents a material with transversely staggered particulates. With focus on low cycle fatigue, the effect of balanced as well as unbalanced cyclic loading is studied.

1 Introduction

For metal matrix composites (MMC) under monotonic tensile loading the failure mechanisms can be divided in three groups, debonding of the matrix-fibre interface, brittle failure of the reinforcements, and ductile matrix failure, as has been discussed by Needleman, Nutt, Suresh, and Tvergaard (1993). Numerical cell-model studies accounting for these failure mechanisms have been carried out by a number of authors, in order to obtain a parametric understanding of the effect of different material parameters, such as the shape and distribution of fibres, the fibre volume fraction, and the matrix material parameters [Nutt and Needleman (1987); Tvergaard (1990, 1993, 1995, 1998); Llorca, Needlemann, and Suresh (1991); Llorca, Suresh, and Needlemann (1992)].

For cyclic loading the fatigue behaviour of discontinuously reinforced metal matrix composites has been discussed by Allison and Jones (1993), with focus on aluminium based composites. Also Llorca and Poza (1995) have tested SiC particulate reinforced Al under fatigue loading, and Llorca, Suresh, and Needlemann (1992) have used a material model for ductile failure in unit cell analyses to represent damage development during cyclic deformation in metal matrix composites. Recently Pedersen and Tvergaard (1999) have modelled the cyclic plasticity of an aluminium reinforced by short SiC fibres by using a material model that combines isotropic and kinematic hardening with continuum damage mechanics [Lemaitre (1992)]. This nonlinear kinematic hardening rule uses a superposition of isotropic hardening and kinematic hardening [Lemaitre and Chaboche (1990)], which makes it possible to describe the Bauchinger effect, cyclic hardening and softening, ratchetting, and mean stress relaxation. The model has been employed by Pedersen (2000, 1999) to study fatigue damage in cold-forging tools.

In the present paper the approach used in Pedersen and Tvergaard (1999) is applied to analyse the evolution of fatigue damage in a tool-steel metal matrix discontinuously reinforced with TiC particulates, as the material studied in Srivatsan, Annigeri, and Prakash (1997).

2 Cyclic Plasticity Model with Fatigue Damage

The analyses in the present work are based on a small strain formulation of the field equations. The total strain increment is given by the sum of the elastic and plastic parts, $\dot{\varepsilon}_{ij} = \dot{\varepsilon}^e_{ij} + \dot{\varepsilon}^p_{ij}$. The elastic stress strain relationship is described by Hooke's law, $\dot{\sigma}_{ij} = L_{ijkl}\dot{\varepsilon}^e_{kl}$, where the summation convention is adopted for repeated indices, σ_{ij} is the stress tensor, E is Young's modulus and ν is Poisson's ratio.

The plastic strain increment follows the normality rule, $\dot{\varepsilon}^p_{ij} = (\partial f/\partial\sigma_{ij})\,\dot{\lambda}$, where the plastic multiplier, $\dot{\lambda}$, is obtained from the consistency condition, $\dot{f} = 0$. A Mises yield surface with mixed hardening is used, as specified by

$$f = \tilde{\sigma}_e - (R + k) = 0 \tag{1}$$

The stress state is described by the effective stress tensor, $\tilde{\sigma}_e = (3\tilde{s}_{ij}\tilde{s}_{ij}/2)^{1/2}$, where $\tilde{s}_{ij} = \tilde{\sigma}_{ij} - 1/3\delta_{ij}\tilde{\sigma}_{kk}$ is the effective stress deviator. Here, $\tilde{\sigma}_{ij} = \sigma_{ij}/(1-D) - X_{ij}$, where D is a scalar describing the amount of damage in a material point [Lemaitre (1992)]. The kinematic hardening is governed by the back stress tensor, X_{ij}, representing the centre of the yield surface in stress space.

The size of the yield surface is described by the scalars R and k . Here, k is a constant and R a variable, which is used for describing the isotropic hardening or softening of the material. The initial conditions of a cyclic hardening material are described by $k = \sigma_y$ and $R = 0$, where σ_y denotes the initial yield stress. The evolution equation for the variable R is described as

$$\dot{R} = b\,(R_\infty(\Lambda, q) - R)\,\dot{\lambda} \tag{2}$$

where b is a material parameter and the value $R_\infty(\Lambda, q)$ represents the limit of isotropic hardening, as described in more detail in Hopperstad, Langseth, and Remseth (1995); Pedersen (2000); Pedersen and Tvergaard (1999). The description of the nonproportionality of the loading path to be used here follows the form suggested by Benallal, Le Gallo, and Marguis (1988).

[1] Department of Solid Mechanics, Technical University of Denmark, Building 404, DK-2800 Lyngby, Denmark.

The kinematic hardening of the material is described by means of the back stress tensor, X_{ij}, which is taken to be the sum of three contributions, in order to enhance the description of the material stress strain response

$$X_{ij} = \sum_{n=1}^{3} X_{ij}^{(n)} \tag{3}$$

For each of the back stress deviators, $X_{ij}^{D(n)}$, an evolution equation is specified of the form Ohno and Wang (1993)

$$\dot{X}_{ij}^{D(n)} = \frac{2}{3}\gamma^{(n)} X_{\infty}^{(n)} \dot{\varepsilon}_{ij}^{p} - \left(\frac{X_e^{(n)}}{X_{\infty}^{(n)}}\right)^{m_n} X_{ij}^{D(n)} \gamma^{(n)} \dot{\lambda} \tag{4}$$

where the effective back stress is $X_e^{(n)} = \left(3/2 X_{pq}^{(n)} X_{pq}^{(n)}\right)^{1/2}$. Further descriptions of the parameters in Eq. 4 and the representation of ratchetting are given in Pedersen (1999); Pedersen and Tvergaard (1999).

The scalar, D , which is incorporated in the constitutive equations as outlined in Lemaitre (1992) is here used to describe the development of fatigue damage in the material. For an undamaged virgin material, $D = 0$, but when the accumulated plastic strain, p , reaches a threshold value, p_d, damage starts developing in the sense of microvoids or microcracks. As it reaches a critical value, D_c, the material has a high density of microcracks that are likely to coalesce into a macrocrack leading to failure of the structural component. The damage development is described by

$$\dot{D} = \frac{Y}{S}\dot{p}\alpha(p), \quad \alpha = \begin{cases} 1, & \text{if } p \geq p_d \\ 0, & \text{if } p < p_d \end{cases} \tag{5}$$

where S is a material parameter describing the energy strength of damage, the effective plastic strain increment is determined as $\dot{p} = \left(2/3\dot{\varepsilon}_{ij}^{p}\dot{\varepsilon}_{ij}^{p}\right)^{1/2}$ and $\dot{p} = \dot{\lambda}/(1-D)$. The strain energy release rate is given by $Y = \sigma_e^2 R_v / \left(2E(1-D)^2\right)$, where the effective stress is denoted σ_e, and the triaxiality of the stress field is accounted for by the parameter R_v, which is here taken to be specified by

$$R_v = \begin{cases} 1 + C\frac{\sigma_{kk}}{\sigma_y}, & \sigma_{kk} \geq 0 \\ \exp\left(C\frac{\sigma_{kk}}{\sigma_y}\right), & \sigma_{kk} < 0 \end{cases} \tag{6}$$

The material parameter C is adjusted to describe the mean stress sensitivity of damage development [Pedersen (2000)]. The final form of the incremental constitutive relations will not be repeated here, but can be found in Pedersen and Tvergaard (1999); Pedersen (2000).

3 Cell Model and Results

The particles are taken to be elastic with Young's modulus E_f and Poisson's ratio ν_f. Furthermore, perfect bonding is assumed between matrix and particles, and the possibility of particle fracture is neglected. Thus, the only type of failure accounted for is the fatigue damage evolution incorporated in the cyclic plasticity law used for the matrix. In the axisymmetric model, described in more detail in Pedersen and Tvergaard (1999); Tvergaard (1990), the fibre volume fraction f is

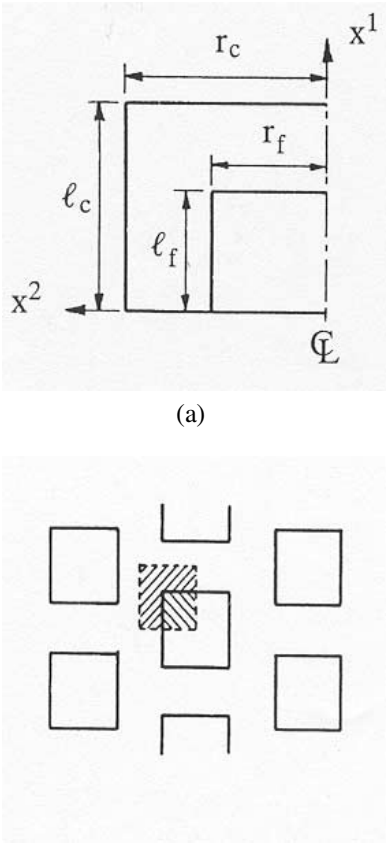

Figure 1 : Periodic arrays of cylindrical particulates with parallel axes. (a) Axisymmetric cell-model. (b) Transversely staggered particulates.

$$f = \frac{r_f^2 l_f}{r_c^2 l_c} \tag{7}$$

Here, l_f and r_f are the fibre half length and radius, respectively, l_c and r_c are the cell length and radius (see Fig. 1), and the aspect ratios of the fibre and cell are

$$\alpha_f = l_f/r_f, \quad \alpha_c = l_c/r_c \tag{8}$$

The major average principal stress σ_1 in the composite is taken to be in the axial direction, and the use of an axisymmetric cell model implies that only cases with a uniform transverse average stress σ_2 are considered. In the cases to be analysed a

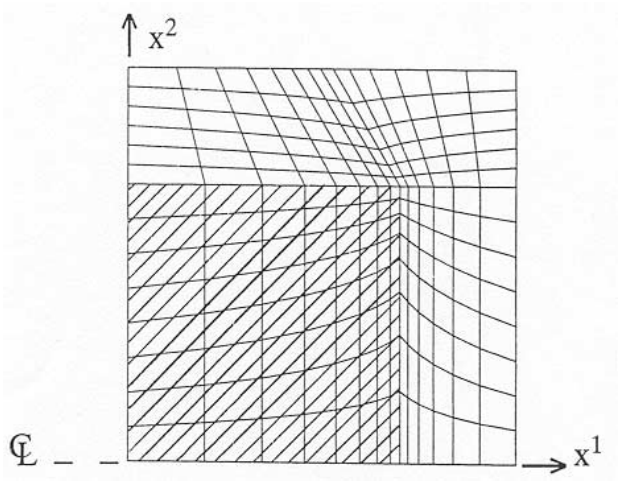

Figure 2 : Mesh used for the numerical computations

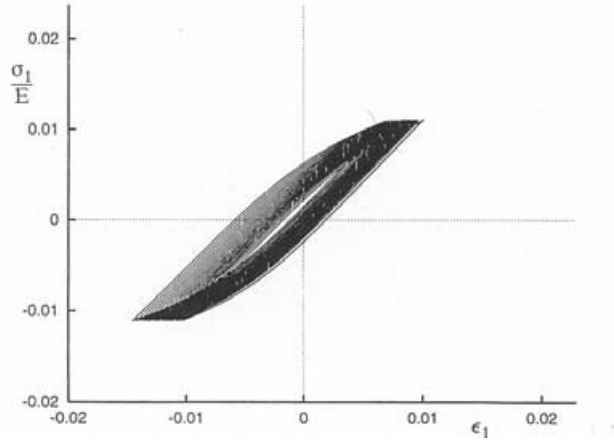

Figure 3 : Overall stress-strain loops for first 20 cycles with balanced stress controlled cycling, $\sigma_{max}/E = -\sigma_{min}/E = 0.011$, and $\rho = 0$.

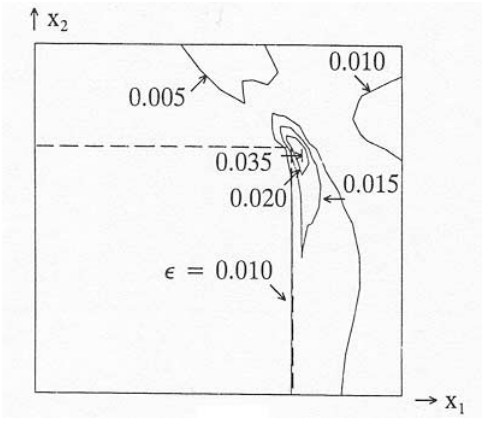

(a)

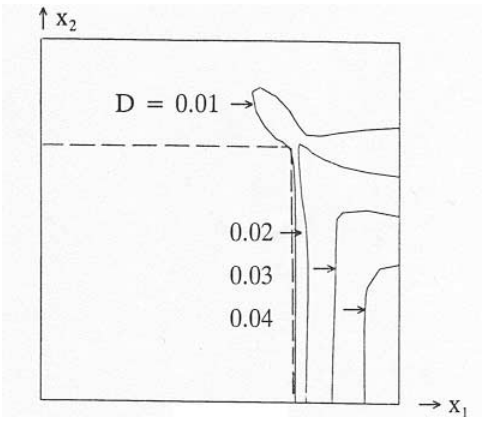

(b)

Figure 4 : Contours of constant strain or damage, at maximum tensile stress, after 20 cycles with balanced stress controlled loading, $\sigma_{max}/E = -\sigma_{min}/E = 0.011$, and $\rho = 0$.

fixed ratio between the axial and transverse average stresses is assumed, $\sigma_2 = \rho\sigma_1$.

In the present analyses the values of the tool-steel material parameters are chosen equal to those determined by Pedersen [Pedersen (2000, 1999)] for Calmax, i.e. $k/E = 0.0054$, $\nu = 0.3$, $b = 1.1$, $R_\infty/E = 0$, $R_0/E = 0.0006$, $\alpha_R = 0.7$, $\beta_R = 160$, $\gamma_R = 0.5$, and $C_q = 0.5$. Furthermore, in the back-stress evolution equations [Eq. 3-4] the parameter values used are $\gamma^1 = 2000$, $\gamma^2 = 180$, $\gamma^3 = 50$, $X^1_\infty/E = 0.00125$, $X^2_\infty/E = 0.00375$, $X^3_\infty/E = 0.001$, $m_1 = 0$, $m_2 = 0$, and $m_3 = 0$. In the damage evolution equations [Eq. 5-6] the parameter values are $S/E = 0.000914$, $p_d = 0$, $D_c = 1.0$ and $C = 0.5$. Furthermore, the elastic constants of the TiC fibres are specified by $E_f/E = 2.185$ and $\nu_f = 0.199$ [see Srivatsan, Annigeri, and Prakash (1997)].

In all the cases to be analysed here the particulates are taken to be periodically distributed in the material and transversely staggered (Fig. 1), as described in Pedersen and Tvergaard (1999); Tvergaard (1990). The aspect ratios are $\alpha_f = \alpha_c = 1$, and the volume fraction of TiC particulates is taken to be $f = 0.35$, to relate to one of steel matrix composites considered in Srivatsan, Annigeri, and Prakash (1997). In all cases analysed the material is subjected to uniaxial cyclic stress, $\rho = 0$. Fig. 2 shows the mesh used for the numerical analyses, with the hatched region representing the particulate.

Fig. 3 shows the overall stress-strain loops for the first 20 cycles, when the loading is stress controlled with balanced cycling, $\sigma_{max}/E = -\sigma_{min}/E = 0.011$. This is the type of test where strain ratchetting is possible and is in fact rather commonly observed [Allison and Jones (1993)], and also Fig. 3 shows ratchetting, since clearly the mean strain moves a small step in the negative direction for each cycle.

The corresponding distributions of the maximum principal

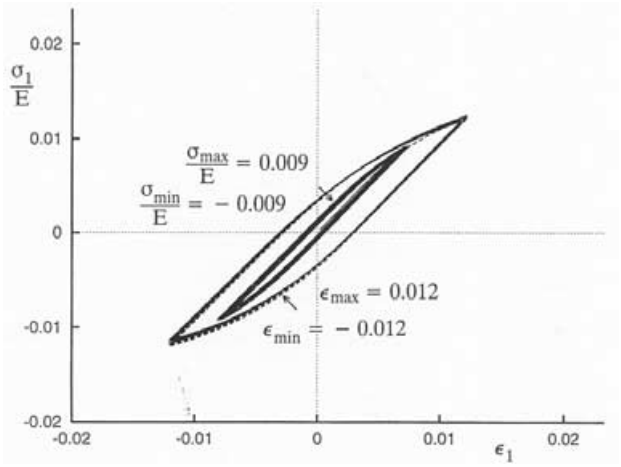

Figure 5 : Overall stress-strain loops for first 20 cycles, corresponding to loading cases with $\rho = 0$. Balanced stress controlled cycling with $\sigma_{max}/E = -\sigma_{min}/E = 0.009$, and balanced strain controlled cycling with $\varepsilon_{max} = -\varepsilon_{min} = 0.012$

strain ε and damage D at the end of cycle no. 20, at maximum tensile stress, are illustrated by the contour curves in Fig. 4. Here, the location of the particulate is indicated by dashed lines. It should be noted that the apparent small amount of damage inside the sharp fibre edge, as indicated in Fig. 4b, is entirely due to a plotting inaccuracy resulting from averaging in the plotting programme. It is seen in Fig. 4a that the strains concentrate at the sharp fibre edge, which results in rapid fatigue damage evolution in the matrix just around the fibre edge. However, the largest amount of damage is found at the bottom right side of Fig. 4b, centrally between two particulate ends. This distribution of damage is better understood if different fibre spacings are considered, and a study for Aluminium matrix composites has shown that for well separated fibres the highest level of damage along the axis of the cylindrical cell would tend to occur about one fibre radius ahead of the fibre end. It is expected that the interaction of two such regions results in the maximum damage region found in Fig. 4b.

Fig. 5 shows the overall stress-strain loops for the first 20 cycles, corresponding to two different loading cases. One case is stress controlled loading with balanced cycling, $\sigma_{max}/E = -\sigma_{min}/E = 0.009$, i.e. like the case in Fig. 3 but with smaller stress amplitude. It is directly seen that there is less plasticity, and the width of the hysteresis loop is smaller. Fig. 6 gives the corresponding distributions of strain and damage after 20 cycles, showing clearly less strain concentration at the fibre edge in Fig. 6a. The much lower levels of plastic straining after 20 cycles result in much reduced levels of damage, by a factor of about 1/4 , but Fig. 6b shows that the distribution of damage is still much like that in Fig. 4b. The other stress-strain loops in Fig. 5 represent strain controlled loading with balanced cycling, $\varepsilon_{max} = -\varepsilon_{min} = 0.012$, so that in this case the loading

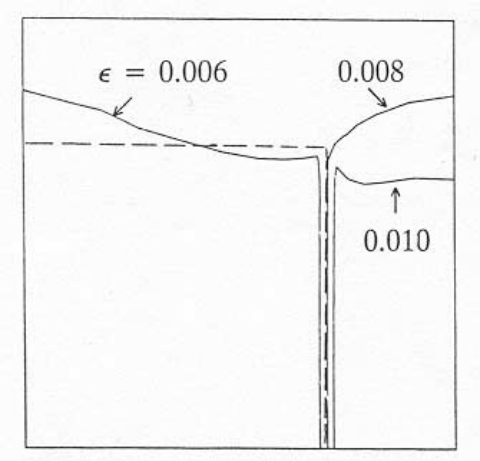

(a)

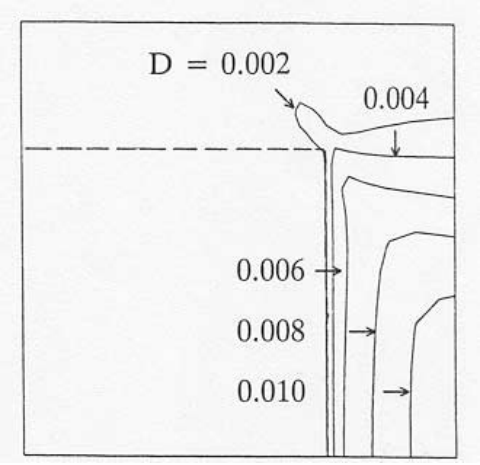

(b)

Figure 6 : Contours of constant strain or damage, at maximum tensile stress, after 20 cycles with balanced stress controlled loading, $\sigma_{max}/E = -\sigma_{min}/E = 0.009$, and $\rho = 0$.

prevents ratchetting. The resulting peak stresses are a little higher than those in Fig. 3, resulting in somewhat higher plastic strains and about twice as high fatigue damage levels after 20 cycles, still with a damage distribution very similar to that in Fig. 4b.

Overall stress-strain loops are shown in Fig. 7 for two cases with unbalanced stress controlled cyclic loading. The stress ranges are the same in both cases, $(\sigma_{max} - \sigma_{min})/E = 0.0208$, but one case has positive mean stress while the other case has negative mean stress. These mean stresses are chosen to give approximately equal amounts of strain ratchetting in positive and negative directions, respectively. Thus, the positive mean stress is numerically larger than the negative mean stress, as would be expected, since zero mean stress gave negative ratch-

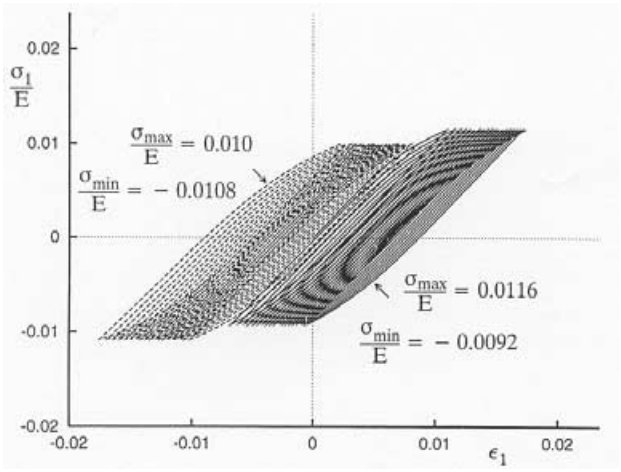

Figure 7 : Overall stress-strain loops for first 20 cycles, corresponding to loading cases with $\rho = 0$ and unbalanced stress controlled loading.

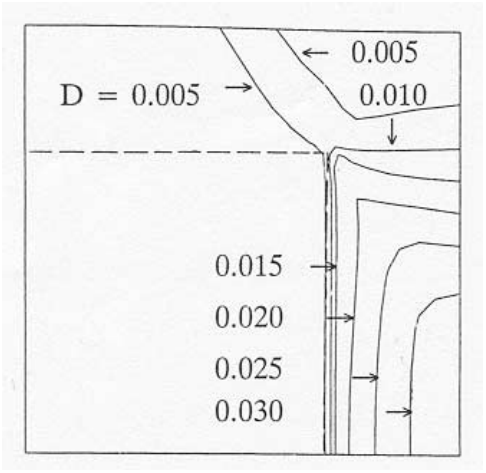

(a)

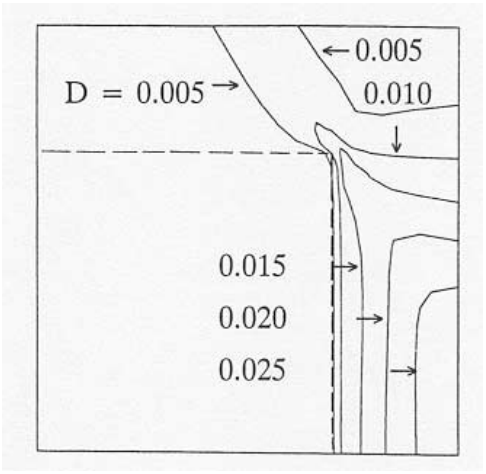

(b)

Figure 8 : Contours of constant damage after 20 cycles with $\rho = 0$ and unbalanced stress controlled loading. (a) $\sigma_{max}/E = 0.0116$, $\sigma_{min}/E = -0.0092$. (b) $\sigma_{max}/E = 0.010$, $\sigma_{min}/E = -0.0108$.

etting in Fig. 3. The amounts of fatigue damage evolution after 20 cycles are compared in Fig. 8. The damage distributions are in both cases rather similar to that shown in Fig. 4b, but the damage levels are somewhat smaller. This agrees with the somewhat smaller stress range in Figs. 7 and 8, as compared to the case of Figs. 3 and 4. It is also noted that the maximum damage level in Fig. 8a is larger than that in Fig. 8b. This is entirely due to the larger mean stress levels in the case of Fig. 8a, which affects the rate of fatigue damage evolution due to the positive value of C in Eq. 6.

It is noted that the parameter values used here to control the rate of fatigue damage evolution are not very accurately determined in Pedersen (2000, 1999) for the tool-steel Calmax. In particular, the most realistic modelling of material behaviour will often require a threshold value of the plastic strain before damage evolution starts [Lemaitre (1992)], i.e. a value $p_d > 0$ in Eq. 5. This would mean that for a reasonably low stress amplitude, with only a small amount of plastic yielding in each cycle, the material could sustain a rather large number of cycles before fatigue failure would be predicted. Also, the value used for C may be too high, but there is no doubt that $C > 0$ is needed to predict the realistic trend in the stress dependence of fatigue damage evolution, as illustrated in Fig. 8.

References

Allison, J. E.; Jones, J. W. (1993): Fatigue behaviour of discontinuously reinforced metal matrix composites. In Suresh, S. e. a.(Ed): *Fundamentals of Metal Matrix Composites*, pp. 269–294, Butterworth- Heinemann, Boston, MA.

Benallal, A.; Le Gallo, P.; Marguis, D. (1988): Cyclic hardening of metals under complex loadings. In *Proc. of MECAMAT*, pp. 361–371, Besancon, France.

Hopperstad, O. S.; Langseth, M.; Remseth, S. (1995): Cyclic stress strain behaviour of alloy AA6060, Part I: Uniaxial experiments and modelling. *Int. Journal of Plasticity*, vol. 11, pp. 725–739.

Lemaitre, J. (1992): *A Course on Damage Mechanics*. Springer-Verlag.

Lemaitre, J.; Chaboche, J.-L. (1990): *Mechanics of Solid Materials*. Cambridge University Press.

Llorca, J.; Needlemann, A.; Suresh, S. (1991): An analysis of the effects of matrix void growth on deformation and ductility in metal-ceramic composites. *Acta Metall. Mater.*, vol. 39, pp. 2317–2335.

Llorca, J.; Poza, P. (1995): Influence of reinforcement fracture on the cyclic stress-strain curve of metal-matrix composites. *Acta Metall. Mater.*, vol. 43, pp. 3959–3969.

Llorca, J.; Suresh, S.; Needlemann, A. (1992): An experimental and numerical study of cyclic deformation in metal-matrix composites. *Metall. Trans.*, vol. 23a, pp. 919–934.

Needleman, A.; Nutt, S. R.; Suresh, S.; Tvergaard, V. (1993): Matrix, reinforcement and interfacial failure. In Suresh, S. e. a.(Ed): *Fundamentals of Metal Matrix Composites*, pp. 233–250, Butterworth- Heinemann, Boston, MA.

Nutt, S. R.; Needleman, A. (1987): Void nucleation at fiber ends in Al-SiC composites. *Scr. Metall.*, vol. 21, pp. 705–710.

Ohno, N.; Wang, J.-D. (1993): Kinematic hardening rules with critical state of dynamic recovery, Part I: Formulation and basic features for ratchetting behaviour. *Int. Journal of Plasticity*, vol. 9, pp. 375–390.

Pedersen, T. Ø. (1999): Numerical studies of low cycle fatigue in forward extrusion dies. *J. Materials Processing Technology, to appear*.

Pedersen, T. Ø. (2000): Numerical modelling of cyclic plasticity and fatigue damage in cold-forging tools. *Int. J. Mech. Sci.*, vol. 42, pp. 799–818.

Pedersen, T. Ø.; Tvergaard, V. (1999): On low cycle fatigue in metal matrix composites. *Int. J. Damage Mechanics*, vol. (to appear), pp. Report, Technical University of Denmark.

Srivatsan, T. S.; Annigeri, R.; Prakash, A. (1997): An investigation of cyclic plastic strain response and fracture behavior of steel-based metal-matrix composites. *Engineering Fracture Mechanics*, vol. 56, pp. 451–481.

Tvergaard, V. (1990): Effect of fibre debonding in a whisker-reinforced metal. *Mater. Sci. Eng.*, vol. A125, pp. 203–213.

Tvergaard, V. (1993): Model studies of fibre breakage and debonding in a metal reinforced by short fibres. *J. Mech. Phys. Solids*, vol. 41, pp. 1309–1326.

Tvergaard, V. (1995): Fibre debonding and breakage in a whisker-reinforced metal. *Materials Science and Engineering*, vol. A190, pp. 215–222.

Tvergaard, V. (1998): Effects of ductile matrix failure in three dimensional analysis of metal matrix composites. *Acta Mater.*, vol. 46, pp. 3637–3648.